Journal of Inorganic Biochemistry 195 (2019) 174–181

Contents lists available at ScienceDirect

Journal of Inorganic Biochemistry

journal homepage: www.elsevier.com/locate/jinorgbio

Design, synthesis and biological evaluation of cobalt(II)-Schiff base complexes as ATP-noncompetitive MEK1 inhibitors

Hongyue Li, Dandan Xi, Yan Niu, Chao Wang, Fengrong Xu, Lei Liang*, Ping Xu*

Department of Medicinal Chemistry, School of Pharmaceutical Sciences, Peking University Health Science Center, 38 Xueyuan Road, Beijing 100191, China

ARTICLE INFO

Keywords:
Cobalt(II)-Schiff base complexes
ATP-noncompetitive MEK1 inhibitors
Molecular docking

ABSTRACT

In this report, we designed and synthesized a series of cobalt(II)-Schiff base complexes (CoSBC) with competent MEK1 (mitogen-activated protein kinase kinase − 1) inhibitory activity. Based on our previous report, the CoSBC exhibited high binding affinity with MEK1 protein. To further explore metal complexes as MEK1 inhibitors, a series of transition metals and ligands were employed to build a library of various metal Schiff base complexes. The MEK inhibition assays revealed that only CoSBC exhibited obvious inhibitory activity, complex **2b** showed the best inhibition both in BRaf (B-rapidly accelerated fibrosarcoma)/MEK1 and MEK1/ERK2 (extracellular signal-regulated kinases-2) cascading (IC_{50} is 1.988 ± 0.14 μM and 1.589 ± 0.054 μM respectively). In addition, homogeneous time-resolved fluorescence test method was used to prove that CoSBC as ATP-noncompetitive MEK1 inhibitor. MEK kinase selectivity assay indicated that CoSBC can selectively inhibit MEK1/2 kinases rather than other MAPKs (mitogen-activated protein kinases) family kinases. Moreover, the interaction mode of **2b** with MEK1 protein has been demonstrated by computer aided drug design.

1. Introduction

Mitogen-activated protein kinase (MAPK) is an important protein kinase found in the mid-1980s and is an important core signaling pathway in cells. The MAPK pathway is mainly divided into four subfamilies including extracellular signal-regulated kinase (ERK) pathway, c-Jun NH2-terminal kinase (JNK) pathway, p38 pathway and ERK5 (extracellular signal-regulated kinases-5) pathway [1]. The Ras (a class of protein called small GTPase)/Raf/MEK/ERK signaling pathway (also known as MAPK/ERK pathway) (Fig. 1) is responsible for the coordination and regulation of cell growth and differentiation in response of extracellular stimulations [2–4]. MEK (mitogen-activated protein kinase kinase), as a pivotal node in this pathway, is activated by Raf (rapidly accelerated fibrosarcoma), which including A-, B- and C-rapidly accelerated fibrosarcoma (ARaf, BRaf and CRaf) three subtypes, and located in the downstream of it. Complete the process from inactivity to phosphorylation. MEK1 and MEK2 are dual specificity kinases and responsible for the phosphorylation and activation of the ERK1 and ERK2. Subsequently, activated ERK1/2 can translocate to the nucleus and phosphorylate additional transcription factors. These series of activities regulate multiple cellular events including proliferation, survival and differentiation, etc.

The abnormal activation of this pathway is closely related to the occurrence and development of many diseases, such as cerebral injury, myocardial hypertrophy, diabetes, inflammation and cancer, among which cancer research is most conducted in-depth [5]. The up-regulation of this pathway is observed in many kinds of tumors including myeloma [6], metastatic biliary carcinoma [7], non-small cell lung cancer and prostate cancer [8], etc. The development of MEK inhibitors has prompted investigations against both this important drug target and the whole pathway [9]. In the past two decades, many small molecular MEK inhibitors have been reported [10]. According to the binding site of inhibitor with MEK protein, it can be classified as ATP competitive MEK inhibitors and ATP noncompetitive MEK inhibitors. However, ATP competitive MEK inhibitors exhibit lower selectivity and more serious toxic side effects than ATP noncompetitive inhibitors. Therefore, the latter one is more popular.

To date, three of them have been approved by FDA (food and drug administration), namely Trametinib [11] (in 2013), Cobimetinib [12] (in 2015) and Binimetinib (in 2018, combined with Encorafenib) for the treatment of advanced melanoma. Besides, Selumetinib has been granted Orphan Drug Designation for the treatment of differentiated thyroid cancer [13] (Fig. S1). Therefore, finding MEK inhibitors has important significance and prospects for the treatment of diseases.

To our knowledge, the successful clinical application of inorganic drugs, such as platinum(II) chemotherapeutics and gold-containing

* Corresponding authors.
E-mail addresses: leiliang@bjmu.edu.cn (L. Liang), pingxu@bjmu.edu.cn (P. Xu).

https://doi.org/10.1016/j.jinorgbio.2019.03.022
Received 16 November 2018; Received in revised form 22 March 2019; Accepted 27 March 2019
Available online 30 March 2019
0162-0134/

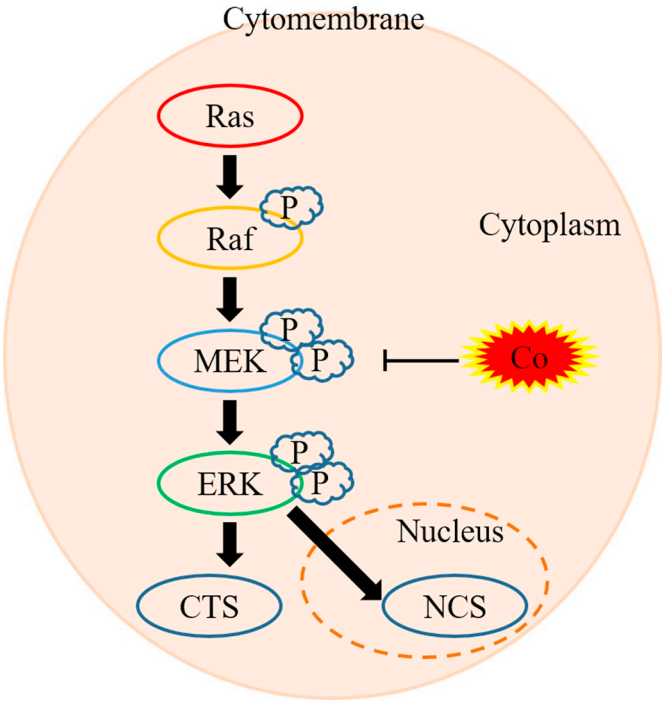

Fig. 1. Components and functions of ERK signaling pathway interfered by cobalt complex. P: phosphorylation, Co: CoSBC, CTS: cytosolic substrates, NCS: nuclear substrate.

antiarthritic agents, have significantly promoted the development of transition metals in medicine [14]. Among transition metals, cobalt has unique physical and chemical properties, it can adopt a wide variety of coordination ligands, geometries and oxidation states. These characters make cobalt can be manipulated to potential drug candidates [15]. Moreover, cobalt plays a key role in composing vitamin B_{12} [16] and cobalt nitrilehydratases [17]. It also displays diverse properties as cobalt complexes in antitumor [18,19], antiviral [20,21] and antimicrobial [22–24] drug candidates. However, cobalt(II)-Schiff base complexes (CoSBC) used as MEK inhibitors has been scarcely reported [9].

According to our previous report, the CoSBC exhibited high binding affinity with MEK1 protein [9]. However, it is not clear that if this kind of compounds exhibit MEK1 kinase inhibition and the mode of action. Herein, we design and synthesize a series of metal complexes to explore that question. Homogeneous time-resolved fluorescence assay (HTRF) technical method was used to test molecular level MEK1 inhibitory activity. The mechanism by which CoSBC inhibits MEK1 kinase was studied and docking study was used to mimic the CoSBC-MEK1 protein binding mode. The finding of this study will promote the discovery of novel MEK1 targeted inhibitors and investigation of the target ability of MEK1 allosteric binding site.

2. Results and discussion

2.1. Chemistry

The structures and synthetic procedures of the target compounds were outlined in Scheme 1. Different diamines were dissolved in methanol and reacted with a series of substituted salicylaldehydes or pyridine salicylaldehydes to prepare organic ligands [25–33]. Then the metal complexes were prepared according to literatures [25–33].

2.2. Biological evaluation

2.2.1. In vitro MEK1 inhibition and structure activity relationship (SAR) analysis

The metal complexes and selected Schiff base ligands were tested with enzyme-based assays for their MEK inhibitory properties. **Trametinib** (approved by FDA in 2013) and **U0126** which are recognized allosteric MEK1 inhibitors reported before were used as the positive controls. Most of the CoSBC showed promising inhibitory potencies both in BRaf/MEK1 and MEK1/ERK2 cascading and also better ligand efficiency (LE) than **U0126** (Table 1). Meanwhile, none of the Schiff base ligands showed inhibitory potencies in either BRaf/MEK1 and MEK1/ERK2 cascading (Tables S1). Continuous assays were then performed to determine the IC_{50} values of the selected candidates (inhibition ratio > 90% at 10 μM). As listed in Table 1, most of the CoSBC exhibited inhibitory activity both in BRaf/MEK1 and MEK1/ERK2 cascading at micromolar range. Comparing **2a–2c**, introduction of hydroxyl (**2d–f**) group to the salicylaldehyde moiety showed no enhancement of the MEK inhibition activity. Nevertheless, replacing cobalt(II) by other transition metals such as copper(II), zinc(II), nickel(II), manganese(II), iron(II) (**3a-c, 4a-c, 5a-c**) resulted in complete loss of activity. Most of the complexes containing halogen(s) (**2 g-s**) showed low activity, except **2 s** which exhibited good inhibitory activity in MEK1/ERK2 cascading. Moreover, bulk diamine moiety showed negative effect to the activity. For instance, complex (**2t**) showed less activity. In addition, when the Schiff base ligand was substituted by electron withdrawing group (**2u**), the inhibitory activity also disappeared. It is noteworthy that tetradentate NNOO moiety is vital as the central metal. For example, tetradentate NNNN ligand was used to replace the NNOO analog (**9a–b**) and the MEK1 inhibitory activity disappeared. Above all, compared **2b** (IC_{50} = 1.589 ± 0.054 μM, LE is 0.32) and positive control **U0126** (IC_{50} = 24.03 ± 5.80 μM, LE is 0.24), the inhibitory activity of **2b** is higher in MEK1/ERK2 cascading and exhibited a better ligand efficiency. But is not higher than positive drug **Trametinib** (IC_{50} = 0.069 ± 0.13 μM, LE is 0.27), however, the structural types of this two compounds are completely different and **2b** has a larger LE, indicating that CoSBC also have a large structural modification space to enhance the inhibitory activity.

2.2.2. Effects of ATP concentrations on MEK1 inhibition

To our knowledge, ATP-noncompetitive inhibitors for MEK1 are superior to the ATP-competitive analogs due to their less undesired adverse effects [34]. In order to explore the inhibition mechanism of CoSBC, ATP competitive profiles of these inhibitors were evaluated [35] using representative compound **2l** and **2n** in BRaf/MEK1 cascading inhibition assay by changing concentrations of ATP (Fig. 2). The IC_{50} values were 3.450 μM, 1.921 μM and 1.749 μM for **2l**, and 4.407 μM, 1.311 μM and 2.105 μM for **2n**, respectively when the ATP concentration varied from 33.33 μM to 100 μM and 300 μM. No increase in IC_{50}s was noticed even when ATP concentration was increased up to 300 μM, and it suggested that CoSBC inhibited the BRaf/MEK1 assay in an ATP non-competitive manner rather than ATP-competitive inhibitors.

2.2.3. Effects of ERK concentrations on MEK1 inhibition

Since **2 s** exhibited the most potent inhibition in MEK1/ERK2 cascading, it was further used to examine the effects on phosphorylated MEK1 kinase in different concentrations of ERK2. We tested the IC_{50} of **2s** in presence of different concentrations of ERK2 (20 nM, 40 nM and 80 nM). As shown in Fig. 3, the IC_{50} values are 1.293 μM, 1.206 μM and 1.363 μM respectively, did not show a difference of > 10 μM. The results indicating MEK1 inhibition of the CoSBC may not mediated by binding to ERK and pointing to these complexes probably located in the allosteric pocket of MEK1.

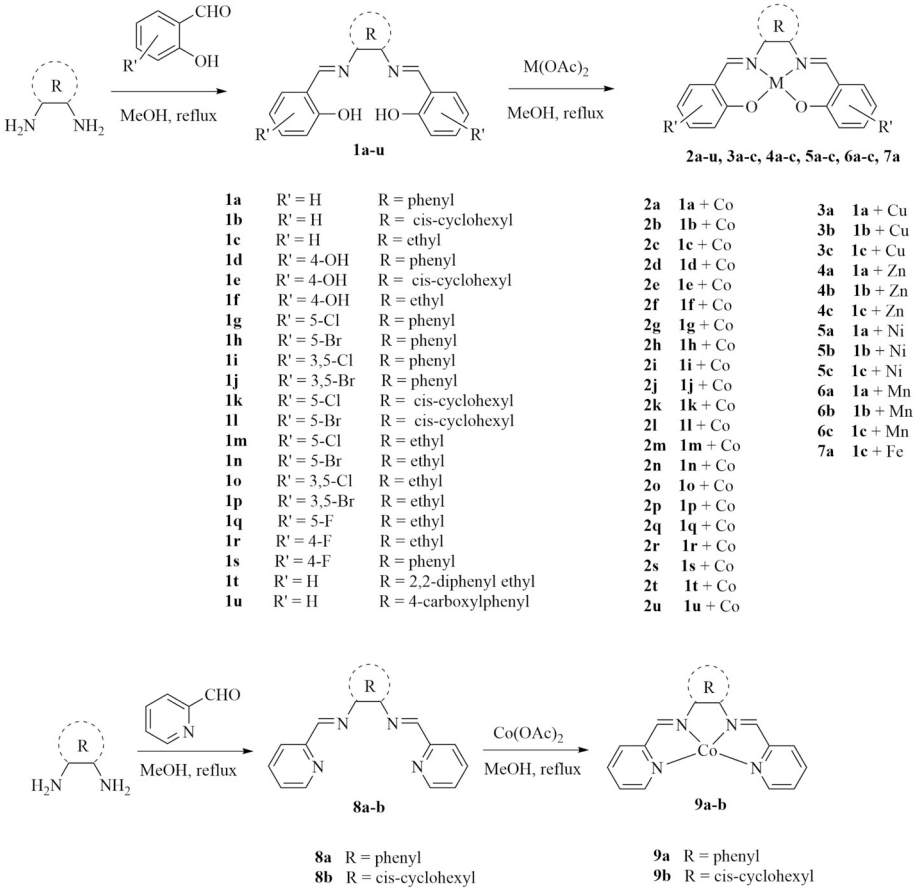

Scheme 1. Synthetic route of ligands and metal complexes.

Table 1
Structure, in vitro enzymatic inhibitory activity and ligand efficiency of metal complexes.

Compd.	BRaf/MEK1[a] -IC_{50}(μM)	MEK1/ERK2[a] -IC_{50}(μM)	LE[b]	Compd.	BRaf/MEK1[a] -IC_{50}(μM)	MEK1/ERK2[a] -IC_{50}(μM)	LE[b]
Trametinib	0.00048 ± 0.08	0.069 ± 0.13	0.27	**2r**	> 10	> 10	n.t.
U0126	0.20 ± 0.012	24.03 ± 5.80	0.24	**2s**	6.56 ± 0.849	1.19 ± 0.023	0.30
2a	2.01 ± 0.073	1.59 ± 0.337	0.32	**2 t**	7.72 ± 2.59	7.70 ± 2.184	0.21
2b	1.99 ± 0.14	1.59 ± 0.054	0.32	**2u**	> 10	> 10	n.t.
2c	6.54 ± 0.45	2.41 ± 0.438	0.37	**3a**	> 10	> 10	n.t.
2d	2.82 ± 1.59	1.58 ± 0.52	0.29	**3b**	> 10	> 10	n.t.
2e	2.95 ± 1.98	4.61 ± 0.21	0.27	**3c**	> 10	> 10	n.t.
2f	2.19 ± 0.77	3.11 ± 1.165	0.33	**4a**	> 10	> 10	n.t.
2g	> 10	5.57 ± 1.898	0.27	**4b**	> 10	> 10	n.t.
2h	> 10	6.61 ± 0.097	0.26	**4c**	> 10	> 10	n.t.
2i	> 10	> 10	n.t.	**5a**	> 10	> 10	n.t.
2j	> 10	> 10	n.t.	**5b**	> 10	> 10	n.t.
2k	2.27 ± 0.195	6.30 ± 0.798	0.26	**5c**	> 10	> 10	n.t.
2l	2.41 ± 0.877	4.24 ± 0.180	0.27	**6a**	> 10	> 10	n.t.
2 m	1.84 ± 0.169	2.06 ± 0.155	0.34	**6b**	> 10	> 10	n.t.
2n	2.93 ± 1.743	2.63 ± 0.692	0.33	**6c**	> 10	> 10	n.t.
2o	> 10	> 10	n.t.	**7a**	> 10	> 10	n.t.
2p	> 10	> 10	n.t.	**9a**	> 10	> 10	n.t.
2q	> 10	> 10	n.t.	**9b**	> 10	> 10	n.t.

n.t.: not tested. [a] Values represent the mean ± SD determined in three independent experiments, each based on three biological replicates. [b] LE: Ligand efficiency (in kcal mol^{-1} $atom^{-1}$) was calculated as $LE = 1.37 \times (-\log IC_{50})/N$. IC_{50} in M and MEK/ERK cascading IC_{50} was used, N is the number of non-hydrogen atoms.

2.3. Docking study

Computer aided drug design (CADD) was used to mimic the interaction of the CoSBC with MEK1 protein. As shown in Fig. 4, the docking results provides us some information as (1) One benzene ring of the Schiff base ligand occupies the hydrophobic pocket surrounded by Met 144, Phe 210 and Ile 142 snugly, stabilizing π-π stacking with Phe 210. (2) The Schiff base ligand provides two oxygen anion, building a salt bridge with the key amino acid Lys 98. It was calculated that the distance between O^- and Lys 98 is 2.14 Å. (3) Besides, Co^{2+} has a salt bridging effect with Asp 209 as the distance between Co^{2+} and oxygen of carbonyl of Asp 209 is 2.36 Å, indicating it may be coordinate covalent bonds. (4) In addition, the dihedral angle between the salt bridge and the CoSBC is calculated as 79.8° and 81.4°, closed to the

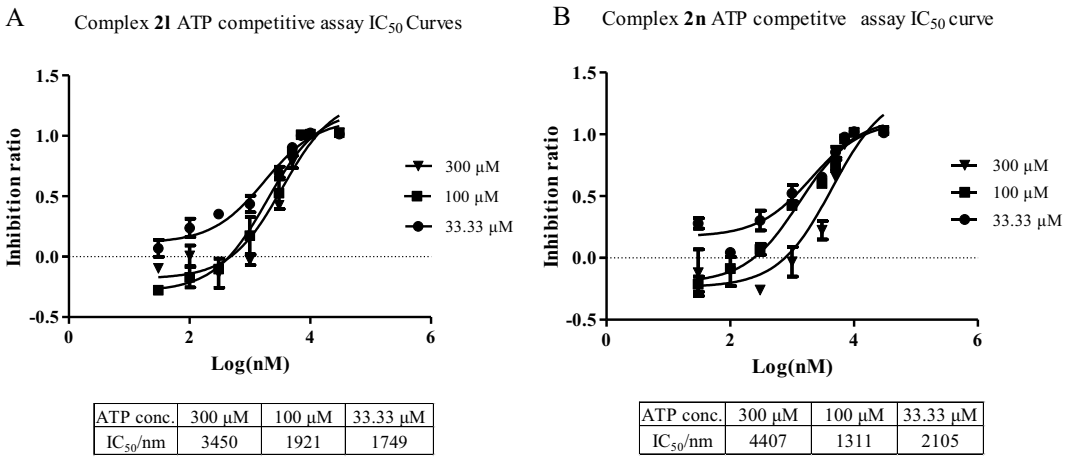

ATP conc.	300 μM	100 μM	33.33 μM
IC_{50}/nm	3450	1921	1749

ATP conc.	300 μM	100 μM	33.33 μM
IC_{50}/nm	4407	1311	2105

Fig. 2. Dose-response curves of (A) complex **2l** and (B) complex **2n** in ATP competition assay.

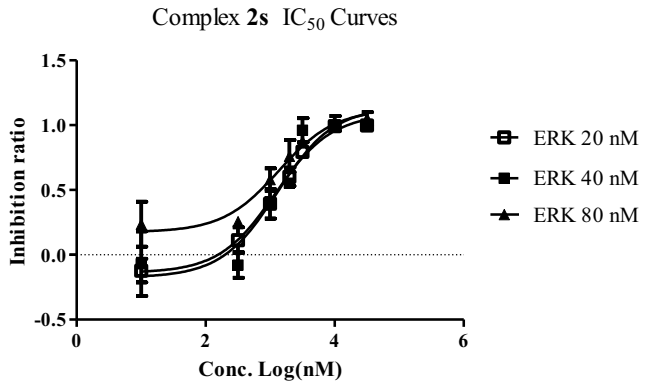

ERK conc.	20 nM	40 nM	80 nM
IC_{50}/nm	1293 nM	1206 nM	1363 nM

Fig. 3. Dose-response curves of complex **2s** in ERK competition assay.

right angle (Fig. 5). Since Co(II) favorably forms quadridentate and hexa-coordinate coordination structure by its valence, the two axial coordination of cobalt(II) Schiff base complex can be easily bounded to oxygen of the carbonyl of Asp 209 [25]. We hypothesis that the tunable coordination of cobalt Schiff base complex and its flexibility based on the appropriate radius of cobalt cation result in its unique MEK1 inhibitory activity rather than other analogues.

2.4. MEK kinase selectivity study

If the designed compounds only produces inhibitory activity against the target pathway kinase and has little effect on other pathways, it will reduce the side effects of the compounds. Therefore, MEK kinase selectivity study is necessary. To elucidate the specificity for MEK kinase of CoSBC, compound **2a** and **2b** were selected to kinase selectivity assay. MEK1/2 inhibitors **U0126**, **PD0325901** and typical metal drug **cisplatin** were used as positive controls (Table 2). All compounds were tested in 10 μM concentration.

12 kinases were selected to detect the inhibitory of MAPK family kinases and mTOR (mammalian target of rapamycin) kinase in PIKK (phosphatidylinositol kinase-related kinase) family associated with the MAPK family. Among the 12 MAPK family kinases, ERK pathway kinases (BRaf, BRaf (V599E), MEK1/2, ERK1/2), JNK pathway kinases (JNK1α1, JNK2α2, JNK3 and MKK4 (mitogen activated-protein kinase kinase-4)), MKK6 (mitogen activated-protein kinase kinase-6) belongs to the p38 pathway and MEKK2 (MEK kinase-2) belongs to the ERK5 pathway. The results show that compounds **2a** and **2b**, as well as **U0126** and **PD0325901**, can significantly inhibit BRaf, BRaf (V599E), MEK1 and MEK2 kinases. The significant inhibitory activity of both the BRaf and BRaf (V599E) kinases is due to the demand of inactive MEK1 as the substrate for the kinase inhibition test. This result is consistent with the results that CoSBC can inhibit both of the BRaf/MEK1 cascading and the MEK1/ERK2 cascading. Furthermore, the MEK1/2 kinase inhibitory activity of **2a** and **2b** are better than **U0126**, and equivalent to **PD0325901**. The results show that **2a** and **2b** exhibit better MEK1/2 selectivity inhibition than other MAPKs family kinases. It is obvious that CoSBC can selectively inhibit BRaf/MEK1 cascading and MEK1/ERK2 cascading (Table 2).

3. Conclusion

In this study, we designed, synthesized a series of cobalt(II)-Schiff base complexes as novel ATP-noncompetitive MEK1 inhibitors. Some candidates (**2a-f**, **2k-n**, **2s-t**) can inhibit both inactive and phosphorylated MEK1 and then activate the downstream substrate ERK2. In order to investigate the SAR of CoSBC, we chose diverse transition metals (Ni, Cu, Zn, Mn, Fe) and/or ligands. However, none of these analogues exhibited MEK1 inhibitory activity. In conclusion, CoSBC can selectively inhibit BRaf/MEK1 cascading and MEK1/ERK2 cascading among 13 kinases. ATP competitive assay and substrate ERK2 competitive assay indicated that CoSBC are probably allosteric MEK1 inhibitors. The detailed mechanistic study of CoSBC as antitumor and antimicrobial agents is ongoing in our laboratory.

4. Experimental section

4.1. Chemicals and instrumentation

All the reagents were commercially available and used without further purification. The positive drug **U0126**, **PD0325901**, **cisplatin** and **Trametinib** were purchased from Selleck Chemicals.

Nuclear magnetic resonance (NMR) spectroscopy was performed on Bruker avance III 400spectrometers. Chemical shifts were reported in parts per million (ppm, δ) relative to tetramethylsilane (0.00 ppm) as the internal standard unless otherwise noted. The coupling constant (J) was reported in Hertz (Hz). Proton coupling patterns were abbreviated as follows; s: singlet, d: doublet, m: multiplet. Data were presented as follows; chemical shift (multiplicity, coupling constant, integration). Low- and high-resolution mass spectra (LRMS and HRMS) were obtained with electrospray ionization (ESI) produced by Waters ACQ-SQDLC–MS spectrometer and Bruker Apex IV FTMS ESI spectrometer, respectively.

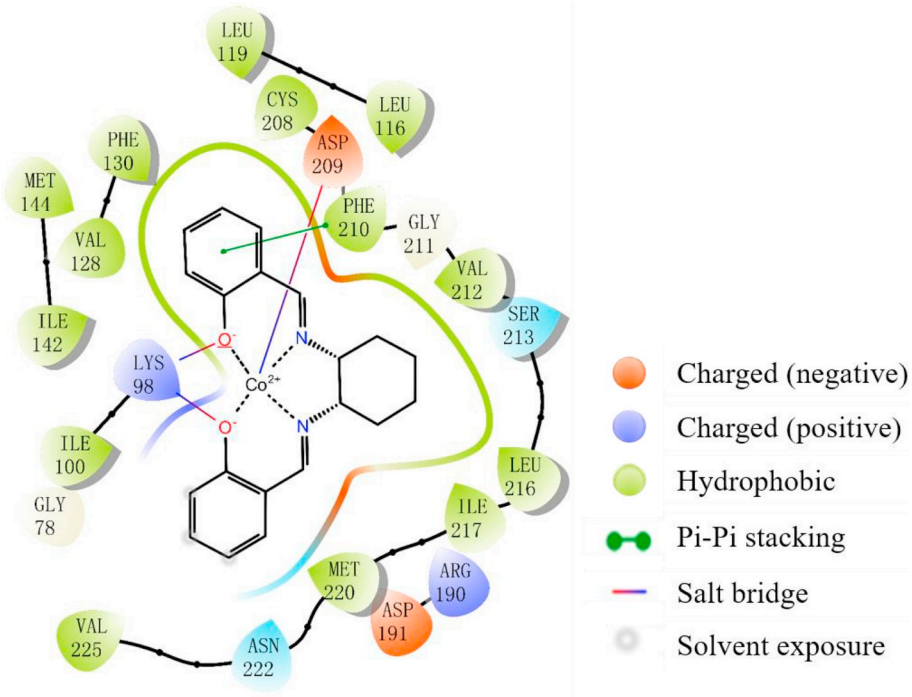

Fig. 4. Cobalt(II)-Schiff base complex (**2b**) with MEK protein (3WIG) docking 2D diagram.

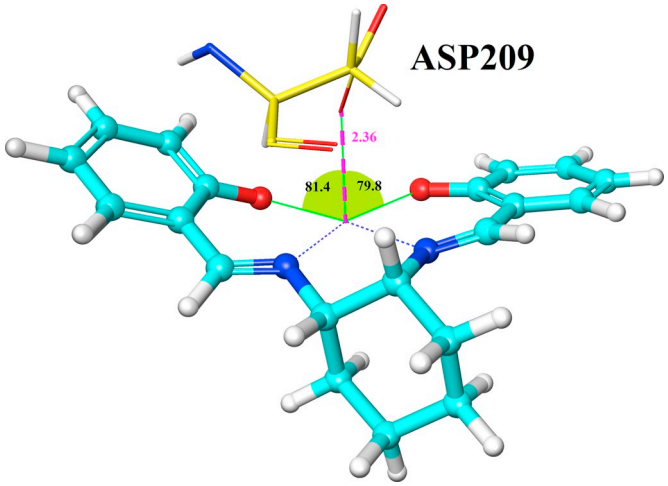

Fig. 5. Location relation between cobalt(II)-Schiff base complex (**2b**) and residue ASP 209.

Table 2
Inhibition activities of selected compounds against 13 kinds of related kinases.

Kinases	Inhibition (%), 10 μM*				
	2a	**2b**	**cisplatin**	**U0126**	**PD0325901**
B-Raf(h)	100	106	43	99	107
B-Raf(V599E)(h)	104	103	5	100	103
JNK1α1(h)	34	49	-1	−3	1
JNK2α2(h)	56	54	8	3	6
JNK3(h)	40	35	−5	2	−8
ERK1(h)	14	36	1	24	21
ERK2(h)	80	67	16	18	7
MEK1(h)	94	84	6	36	98
MEK2(h)	97	89	−9	63	98
MEKK2(h)	25	6	−1	0	−1
MKK4(m)	62	39	−10	−8	−4
MKK6(h)	−1	−2	−3	10	3
mTOR(h)	17	5	−6	0	−7

*The data is the average of two independent replicates. (h) = Human, (m) = Mouse.

4.2. Synthesis and characterization

4.2.1. General procedure for synthesis of Schiff base ligands

A solution of substituted salicylaldehyde (10 mmol) in methanol (20 mL) was added dropwise to a solution of different substituted 1,2-diaminoethane (5 mmol) in methanol (20 mL). The mixture was refluxed for 2 h and the precipitate of Schiff base ligand was obtained as solid product. Then the solid was separated by filtration, washed with cold methanol and dried in vacuum. Finally, it was recrystallized from methanol to yield as pure ligand.

4.2.2. General procedure for synthesis of metal complexes

Corresponding metal salt solution (1 mmol) and Schiff base ligand (1 mmol) were dissolved in methanol (10 mL) and reflux for 1 h. Crystals of the metal complexes were obtained by cooling the reaction mixture.

*4.2.2.1. 2,2′-((1E,1′E)-(1,2-phenylenebis(azanylylidene)) bis (methanylylidene)) diphenol cobalt(II) (**2a**).* Brown solid, yield 62%, mp > 350 °C; IR (KBr, cm^{-1}) $\nu_{(C=N)}$ 1611; HRMS-ESI *m/z* $[M]^+$ calcd for $C_{20}H_{14}CoN_2O_2$: 373.0387, found: 373.0383.

*4.2.2.2. 2,2′-((1E,1′E)-((1R,2S)-cyclohexane-1,2-diylbis (azanylylidene)) bis (methanylylidene)) diphenol cobalt(II) (**2b**).* Red solid, yield 64%, mp 300–301 °C; IR (KBr, cm^{-1}) $\nu_{(C=N)}$ 1604; HRMS-ESI *m/z* $[M]^+$ calcd for $C_{20}H_{20}CoN_2O_2$: 379.0857, found: 379.0851.

*4.2.2.3. 2,2′-((1E,1′E)-(ethane-1,2-diylbis (azanylylidene)) bis (methanylylidene)) diphenol cobalt(II) (**2c**).* Green solid, yield 78%, mp 312–313 °C; IR (KBr, cm^{-1}) $\nu_{(C=N)}$ 1625; HRMS-ESI *m/z* $[M]^+$ calcd for $C_{16}H_{14}CoN_2O_2$: 325.0387, found: 325.0384.

*4.2.2.4. 4,4′-((1E,1′E)-(1,2-phenylenebis (azanylylidene)) bis (methanylylidene)) bis (benzene-1,3-diol) cobalt(II) (**2d**).* Brown solid, yield 38%, mp > 350 °C; IR (KBr, cm^{-1}) $\nu_{(C=N)}$ 1610; HRMS-ESI *m/z*

$[M]^+$ calcd for $C_{20}H_{14}CoN_2O_4$: 405.0286, found: 405.0287.

*4.2.2.5. 4,4′-((1E,1′E)-((1R,2S)-cyclohexane-1,2-diylbis (azanylylidene)) bis (methanylylidene)) bis (benzene-1,3-diol) cobalt(II) (**2e**)*. Brown solid, yield 89%, mp 295–297 °C; IR (KBr, cm^{-1}) $\nu_{(C=N)}$ 1609; HRMS-ESI *m/z* $[M]^+$ calcd for $C_{20}H_{20}CoN_2O_4$: 411.0755, found: 411.0750.

*4.2.2.6. 4,4′-((1E,1′E)-(ethane-1,2-diylbis (azanylylidene)) bis (methanylylidene)) bis (benzene-1,3-diol) cobalt(II) (**2f**)*. Brown solid, yield 38%, mp > 350 °C; IR (KBr, cm^{-1}) $\nu_{(C=N)}$ 1607; HRMS-ESI *m/z* $[M]^+$ calcd for $C_{16}H_{14}CoN_2O_4$: 357.0286, found: 357.0281.

*4.2.2.7. 2,2′-((1E,1′E)-(1,2-phenylenebis (azanylylidene)) bis (methanylylidene)) bis (4-chlorophenol) cobalt(II) (**2g**)*. Black solid, yield 99%, mp > 350 °C; IR (KBr, cm^{-1}) $\nu_{(C=N)}$ 1606; HRMS-ESI *m/z* $[M]^+$ calcd for $C_{20}H_{12}Cl_2CoN_2O_2$: 440.9608, found: 440.9611.

*4.2.2.8. 2,2′-((1E,1′E)-(1,2-phenylenebis (azanylylidene)) bis (methanylylidene)) bis (4-bromophenol) cobalt(II) (**2h**)*. Black solid, yield 91%, mp > 350 °C; IR (KBr, cm^{-1}) $\nu_{(C=N)}$ 1598; HRMS-ESI *m/z* $[M]^+$ calcd for $C_{20}H_{12}Br_2CoN_2O_2$: 528.8598, found: 528.8602.

*4.2.2.9. 6,6′-((1E,1′E)-(1,2-phenylenebis (azanylylidene)) bis (methanylylidene)) bis (2,4-dichlorophenol) cobalt(II) (**2i**)*. Brown solid, yield 97%, mp > 350 °C; IR (KBr, cm^{-1}) $\nu_{(C=N)}$ 1616; HRMS-ESI *m/z* $[M + H]^+$ calcd for $C_{20}H_{11}Cl_4CoN_2O_2$: 509.8907, found: 509.8916.

*4.2.2.10. 6,6′-((1E,1′E)-(1,2-phenylenebis (azanylylidene)) bis (methanylylidene)) bis (2,4-dibromophenol) cobalt(II) (**2j**)*. Black solid, yield 93%, mp > 350 °C; IR (KBr, cm^{-1}) $\nu_{(C=N)}$ 1601; HRMS-ESI *m/z* $[M + H]^+$ calcd for $C_{20}H_{11}Br_4CoN_2O_2$: 685.6886, found: 685.6891.

*4.2.2.11. 2,2′-((1E,1′E)-((1R,2S)-cyclohexane-1,2-diylbis (azanylylidene)) bis (methanylylidene)) bis (4-chlorophenol) cobalt(II) (**2k**)*. Red solid, yield 82%, mp 329–333 °C; IR (KBr, cm^{-1}) $\nu_{(C=N)}$ 1600; HRMS-ESI *m/z* $[M]^+$ calcd for $C_{20}H_{18}Cl_2CoN_2O_2$: 447.0077, found: 447.0081.

*4.2.2.12. 2,2′-((1E,1′E)-((1R,2S)-cyclohexane-1,2-diylbis (azanylylidene)) bis (methanylylidene)) bis (4-bromophenol) cobalt(II) (**2l**)*. Red solid, yield 94%, mp 318–321 °C; IR (KBr, cm^{-1}) $\nu_{(C=N)}$ 1597; HRMS-ESI *m/z* $[M]^+$ calcd for $C_{20}H_{18}Br_2CoN_2O_2$: 534.9067, found: 534.9064.

*4.2.2.13. 2,2′-((1E,1′E)-(ethane-1,2-diylbis (azanylylidene)) bis (methanylylidene)) bis (4-chlorophenol) cobalt(II) (**2m**)*. Brown solid, yield 54%, mp 316–318 °C; IR (KBr, cm^{-1}) $\nu_{(C=N)}$ 1631; HRMS-ESI *m/z* $[M]^+$ calcd for $C_{16}H_{12}Cl_2CoN_2O_2$: 392.9608, found: 392.9606.

*4.2.2.14. 2,2′-((1E,1′E)-(ethane-1,2-diylbis (azanylylidene)) bis (methanylylidene)) bis (4-bromophenol) cobalt(II) (**2n**)*. Brown solid, yield 80%, mp 320–322 °C; IR (KBr, cm^{-1}) $\nu_{(C=N)}$ 1608; HRMS-ESI m/z $[M]^+$ calcd for $C_{16}H_{12}Br_2CoN_2O_2$: 480.8598, found: 480.8593.

*4.2.2.15. 6,6′-((1E,1′E)-(ethane-1,2-diylbis (azanylylidene)) bis (methanylylidene)) bis (2,4-dichlorophenol) cobalt(II) (**2o**)*. Brown solid, yield 92%, mp 289–292 °C; IR (KBr, cm^{-1}) $\nu_{(C=N)}$ 1602; HRMS-ESI *m/z* $[M]^+$ calcd for $C_{16}H_{10}Cl_4CoN_2O_2$: 460.8828, found: 460.8829.

*4.2.2.16. 6,6′-((1E,1′E)-(ethane-1,2-diylbis (azanylylidene)) bis (methanylylidene)) bis (2,4-dibromophenol) cobalt(II) (**2p**)*. Brown solid, yield 91%, mp > 350 °C; IR (KBr, cm^{-1}) $\nu_{(C=N)}$ 1597; LRMS-ESI ($C_{16}H_{10}Br_4CoN_2O_2$) *m/z* 663.6868 $[M + Na]^+$.

*4.2.2.17. 2,2′-((1E,1′E)-(ethane-1,2-diylbis (azanylylidene)) bis (methanylylidene)) bis (4-fluorophenol) cobalt(II) (**2q**)*. Brown solid, yield 11%, mp 321–325 °C; IR (KBr, cm^{-1}) $\nu_{(C=N)}$ 1632; HRMS-ESI *m/z* $[M]^+$ calcd for $C_{16}H_{12}CoF_2N_2O_2$: 361.0199, found: 361.0196.

*4.2.2.18. 6,6′-((1E,1′E)-(ethane-1,2-diylbis (azanylylidene)) bis (methanylylidene)) bis (3-fluorophenol) cobalt(II) (**2r**)*. Brown solid, yield 3%, mp 322–325 °C; IR (KBr, cm^{-1}) $\nu_{(C=N)}$ 1622; HRMS-ESI *m/z* $[M]^+$ calcd for $C_{16}H_{12}CoF_2N_2O_2$: 361.0199, found: 361.0197.

*4.2.2.19. 6,6′-((1E,1′E)-(1,2-phenylenebis (azanylylidene)) bis (methanylylidene)) bis (3-fluorophenol) cobalt(II) (**2s**)*. Brown solid, yield 38%, mp 310–312 °C; IR (KBr, cm^{-1}) $\nu_{(C=N)}$ 1617; HRMS-ESI *m/z* $[M]^+$ calcd for $C_{20}H_{12}CoF_2N_2O_2$: 409.0199, found: 409.0198.

*4.2.2.20. 2,2′-((1E,1′E)-((1,2-diphenylethane-1,2-diyl) bis (azanylylidene)) bis (methanylylidene)) diphenol cobalt(II) (**2t**)*. Red solid, yield 42%, mp 337–340 °C; IR (KBr, cm^{-1}) $\nu_{(C=N)}$ 1603; HRMS-ESI *m/z* $[M]^+$ calcd for $C_{28}H_{22}CoN_2O_2$: 477.1013, found: 477.1018.

*4.2.2.21. 3,4-bis((E)-(2-hydroxybenzylidene) amino) benzoic acid cobalt (II) (**2u**)*. Brown solid, yield 50%, mp 324–326 °C; IR (KBr, cm^{-1}) $\nu_{(C=N)}$ 1615; HRMS-ESI *m/z* $[M]^+$ calcd for $C_{21}H_{14}CoN_2O_4$: 417.0286, found: 417.0282.

*4.2.2.22. 2,2′-((1E,1′E)-(1,2-phenylenebis (azanylylidene)) bis (methanylylidene)) diphenol copper(II) (**3a**)*. Green solid, yield 44%, HRMS-ESI *m/z* $[M + H]^+$ calcd for $C_{20}H_{15}CuN_2O_2$: 378.0430, found: 378.0426.

*4.2.2.23. 2,2′-((1E,1′E)-((1R,2S)-cyclohexane-1,2-diylbis (azanylylidene)) bis (methanylylidene)) diphenol copper(II) (**3b**)*. Brown solid, yield 73%, HRMS-ESI *m/z* $[M + H]^+$ calcd for $C_{20}H_{21}CuN_2O_2$: 384.0899, found: 384.0898.

*4.2.2.24. 2,2′-((1E,1′E)-(ethane-1,2-diylbis (azanylylidene)) bis (methanylylidene)) diphenol copper(II) (**3c**)*. Brown solid, yield 86%, HRMS-ESI m/z $[M + H]^+$ calcd for $C_{16}H_{15}CuN_2O_2$: 330.0430, found: 330.0426.

*4.2.2.25. 2,2′-((1E,1′E)-(1,2-phenylenebis (azanylylidene)) bis (methanylylidene)) diphenol zinc(II) (**4a**)*. Yellow solid, yield 99%, ^1H NMR (400 MHz, DMSO-d_6): δ = 9.02 (s, 2H,N=CH), 6.51–7.92 ppm (m, 12H, Ph); ^{13}C NMR (100 MHz, DMSO-d_6): δ = 172.74, 163.29, 139.84, 136.69, 134.78, 127.71, 123.55, 119.90, 116.94, 113.42 ppm; HRMS-ESI *m/z* $[M + H]^+$ calcd for $C_{20}H_{15}N_2O_2Zn$: 379.0425, found: 379.0419.

*4.2.2.26. 2,2′-((1E,1′E)-((1R,2S)-cyclohexane-1,2-diylbis (azanylylidene)) bis (methanylylidene)) diphenol zinc(II) (**4b**)*. White solid, yield 83%, ^1H NMR (400 MHz, DMSO-d_6): δ = 8.43 (s, 2H,N = CH), 6.41–7.21 (m, 8H, Ph), 3.72 (s, 2H, CH), 1.43–2.03 ppm (m, 8H, CH_2); ^{13}C NMR (100 MHz, DMSO-d_6): δ = 171.46, 167.27, 135.56, 133.23, 123.06, 119.93, 112.57, 62.58, 27.45, 21.62 ppm; HRMS-ESI *m/z* $[M + Cl]^-$ calcd for $C_{20}H_{20}N_2O_2ZnCl$: 419.0505, found: 419.0506.

*4.2.2.27. 2,2′-((1E,1′E)-(ethane-1,2-diylbis (azanylylidene)) bis (methanylylidene)) diphenol zinc(II) (**4c**)*. Yellow solid, yield 93%, ^1H NMR (400 MHz, DMSO-d_6): δ = 8.44 (s, 2H,N = CH), 6.41–7.16 (m, 8H, Ph), 3.73 ppm (s, 4H, CH_2); ^{13}C NMR (100 MHz, DMSO-d_6): δ = 168.46, 155.36, 135.19, 133.24, 123.15, 119.68, 112.63, 56.22 ppm; LRMS-ESI ($C_{16}H_{14}N_2O_2Zn$) *m/z* 330.8770 $[M-H]^-$.

*4.2.2.28. 2,2′-((1E,1′E)-(1,2-phenylenebis (azanylylidene)) bis (methanylylidene)) diphenol nickel(II) (**5a**)*. Red solid, yield 94%, HRMS-ESI *m/z* $[M + H]^+$ calcd for $C_{20}H_{15}NiN_2O_2$: 373.0487, found: 373.0488.

*4.2.2.29. 2,2′-((1E,1′E)-((1R,2S)-cyclohexane-1,2-diylbis (azanylylidene)) bis (methanylylidene)) diphenol nickel(II) (**5b**)*. Red solid, yield 95%, HRMS-ESI *m/z* $[M + H]^+$ calcd for $C_{20}H_{21}NiN_2O_2$: 379.0957, found: 379.0948.

*4.2.2.30. 2,2′-((1E,1′E)-(ethane-1,2-diylbis (azanylylidene)) bis (methanylylidene)) diphenol nickel(II) (**5c**)*. Red solid, yield 71%, HRMS-ESI *m/z* $[M + H]^+$ calcd for $C_{16}H_{15}NiN_2O_2$: 325.0487, found: 325.0484.

*4.2.2.31. 2,2′-((1E,1′E)-(1,2-phenylenebis (azanylylidene)) bis (methanylylidene)) diphenol manganese(II) (**6a**)*. Brown solid, yield 54%, HRMS-ESI *m/z* $[M]^+$ calcd for $C_{20}H_{14}MnN_2O_2$: 369.0436, found: 369.0437.

*4.2.2.32. 2,2′-((1E,1′E)-((1R,2S)-cyclohexane-1,2-diylbis (azanylylidene)) bis (methanylylidene)) diphenol manganese (II) (**6b**)*. Green solid, yield 32%, HRMS-ESI *m/z* $[M]^+$ calcd for $C_{20}H_{20}MnN_2O_2$: 375.0905, found: 375.0900.

*4.2.2.33. 2,2′-((1E,1′E)-(ethane-1,2-diylbis (azanylylidene)) bis (methanylylidene)) diphenol manganese(II) (**6c**)*. Green solid, yield 8%, HRMS-ESI *m/z* $[M]^+$ calcd for $C_{16}H_{14}MnN_2O_2$: 321.0436, found: 321.0431.

*4.2.2.34. 2,2′-((1E,1′E)-(ethane-1,2-diylbis (azanylylidene)) bis (methanylylidene)) diphenol iron (II) (**7a**)*. Black solid, yield 62%, HRMS-ESI *m/z* $[M]^+$ calcd for $C_{16}H_{14}FeN_2O_2$: 322.0405, found: 322.0400.

*4.2.2.35. (N^1E,N^2E)-N^1,N^2-bis (pyridin-2-ylmethylene) benzene-1,2-diamine cobalt(II) (**9a**)*. Pink solid, yield 20%, HRMS-ESI *m/z* [M-Co + H]$^+$ calcd for $C_{18}H_{15}N_4$: 287.1297, found: 287.1293.

*4.2.2.36. (1R,2S,N^1E,N^2E)-N^1,N^2-bis (pyridin-2-ylmethylene) cyclohexane-1,2-diamine cobalt(II) (**9b**)*. Black solid, yield 63%, LRMS-ESI ($C_{18}H_{20}CoN_4$) m/z 351.1104 $[M]^+$.

4.3. Biological assays

Recombinant purified inactive GST-tagged MEK1 and ERK2 protein and recombinant purified active GST-BRAF and GST-MEK1 kinase were purchased from Carna Biosciences Inc., Japan. Polyclonal anti-phospho MEK1/2(Ser217/221)-cryptate, mAb anti-phospho p44/42 MAPK (Thr202/Tyr204)-cryptate and mAb anti GST-XL665 antibodies were purchased from Cisbio Bioassays. All the synthesized derivatives were tested for MEK inhibitory potency in BRaf/MEK1 and MEK1/ERK2 cascade assay. The positive control **Trametinib** and **U0126** were purchased from Selleck Chemicals.

All assays were conducted following the general protocol as below [35,36]:

The homogeneous time resolved fluorescence (HTRF) assay was performed on a Proxiplate-384 F plus solid white plate (Greiner) with 2 μL kinase (0.44 ng/μL BRaf or 0.5 ng/μL active MEK1), 2 μL substrate (30 nM inactive MEK1 or 40 nM ERK2), 2 μL (100 μM) ATP and 4 μL test compound at a variety of concentrations, which were incubated at room temperature for 2 h. Then add 10 μL of the detection buffer which contain 200× polyclonal anti-phospho MEK1/2 (Ser217/221)-cryptate (or mAb anti-phospho p44/42 MAPK (Thr202/Tyr204)-cryptate) and 26 nM mAb anti GST-XL665 incubated at room temperature for 3 h. Finally, the fluorescence signals are detected with FlexStation 3 Multi-Mode Microplate Reader (Molecular Devices, USA). This energy transfer is detected by an increase in the fluorescence emission of the tracer at 668 nm and a decrease in the fluorescence emission of europium at 620 nm. Using the following formula to calculate the inhibition rate:

$$\text{Inhibition\%} = (R_n - R_c)/(R_n - R_b) \times 100\%$$

in which R_n is negative control, R_c is compound signal and R_b is blank control. The curve-fitting software GraphPad Prism was used to generate the curves and determine the IC_{50} values for individual compounds tested. Values represent the mean ± SD determined in three independent experiments, each based on three biological replicates.

4.4. Molecular docking

To explore the binding mode of active compound with MEK1, the module Glide of Schrödinger (LLC, New York, NY, USA) software was used for docking [37]. The default parameter settings were adopted. The three-dimensional (3D) structure of MEK1 (PDB ID: 3WIG) was downloaded from Protein Data Bank (PDB).

4.5. Kinase selectivity assay

The selectivity of representative compound **2a** and **2b** against MEK1 and related pathway kinase were tested by Eurofins using KinaseProfiler™ Service Assay [38]. See the Supplementary Information for detailed protocols.

Abbreviations

CoSBC	Cobalt(II)-Schiff base complexes
DMSO	Dimethyl sulfoxide
ERK	Extracellular signal-regulated kinases
ESI	Electrospray ionization
FDA	Food and drug administration
HRMS	High-resolution mass spectra
HTRF	Homogeneous time resolved fluorescence
Hz	Hertz
JNK	c-Jun NH2-terminal kinase
LE	Ligand efficiency
LRMS	Low-resolution mass spectra
MAPKs	Mitogen-activated protein kinases
MEK	Mitogen-activated protein kinase kinase
MEKK2	MEK kinase-2
MKK	Mitogen activated-protein kinase kinase
MS	Mass spectrum
mTOR	Mammalian target of rapamycin
NMR	Nuclear magnetic resonance
PDB	Protein Data Bank
Ph	Phenyl
PIKK	Phosphatidylinositol kinase-related kinase
ppm	Parts per million
Raf	Rapidly accelerated fibrosarcoma
Ras	a class of protein called small GTPase
SAR	Structure activity relationship

Acknowledgments

This work was supported by the Beijing Natural Science Foundation (7162110), Interdisciplinary Medicine Seed Fund of Peking University (BMU2018MC004) and the National Natural Science Foundation of China (21807006/81872731). The authors would also acknowledge Prof. Zhenjun Yang and Prof. Liangren Zhang for kindly providing space and suggestions on bio-experiments.

Conflict of interest

The authors confirm that this article content has no conflict of interests.

Appendix A. Supplementary data

Supplementary data to this article can be found online at https://doi.org/10.1016/j.jinorgbio.2019.03.022.

References

[1] L.F. Chang, A.D. Sharrocks, A. Whitmarsh, Nature 410 (2001) 37–40.
[2] N.G. Ahn, R. Seger, R.L. Bratlien, C.D. Diltz, N.K. Tonks, E.G. Krebs, J. Biol. Chem. 266 (1991) 4220–4227.
[3] W. Kolch, Expert. Opin. Pharmacother. 3 (2002) 709–718.
[4] H.J. Schaeffer, M.J. Weber, Mol. Cell. Biol. 19 (1999) 2435–2444.
[5] R. Roskoski, Pharmacol. Res. 66 (2012) 105–143.
[6] R. Pinto, S. Herold, et al., Antivir. Res. 92 (2011) 45–56.
[7] T. Bekaii-Saab, M.A. Phelps, et al., J. Clin. Oncol. 29 (2011) 2357–2363.
[8] J.L. Bromberg-White, N.J. Andersen, et al., Brief. Funct. Genomics 11 (2012) 300–310.
[9] H. Li, T. Zhou, H. Liu, et al., Bioorg. Med. Chem. Lett. 27 (2017) 2221–2224.
[10] S. Price, Expert Opin. Ther. Pat. 18 (2008) 603–627.
[11] D.E. Uehling, P.A. Harris, Bioorg. Med. Chem. Lett. 25 (2015) 4047–4056.
[12] K.D. Rice, N. Aay, et al., ACS Med. Chem. Lett. 3 (2012) 416–421.
[13] Y.T. Patel, V.M. Daryani, et al., CPT Pharmacometrics Syst. Pharmacol. 6 (2017) 305–314.
[14] T.W. Hambley, Dalton Trans. 21 (2007) 4929–4937.
[15] M.C. Heffern, N. Yamamoto, R.J. Holbrook, et al., Curr. Opin. Chem. Biol. 17 (2013) 189–196.
[16] R. Banerjee, S.W. Ragsdale, Annu. Rev. Biochem. 72 (2003) 209–247.
[17] T. Yano, T. Ozawa, H. Masuda, Chem. Lett. 37 (2008) 672–677.
[18] D.C. Ware, B.D. Palmer, W.R. Wilson, et al., J. Med. Chem. 36 (1993) 1839–1846.
[19] I. Ott, K. Schmidt, B. Kircher, et al., J. Med. Chem. 48 (2005) 622–629.
[20] V. Groupe, C. Engle, P.E. Gaffney, J. Bacteriol. 4 (1955) 623–624.
[21] J.B. Delehanty, J.E. Bongard, D. Thach, Bioorg. Med. Chem. 16 (2008) 830–837.
[22] M.N. Patel, M.R. Chhasatia, D.S. Gandhi, Bioorg. Med. Chem. Lett. 19 (2009) 2870–2873.
[23] E.K. Efthimiadou, A. Karaliota, G. Psomas, Bioorg. Med. Chem. Lett. 18 (2008) 4033–4037.
[24] L.A. Saghatforoush, F. Chalabian, A. Aminkhan, et al., Eur. J. Med. Chem. 44 (2009) 4490–4495.
[25] T. Joseph, S.B. Halligudi, C. Satyanarayan, et al., J. Mol. Catal. A Chem. 168 (2001) 87–97.
[26] S. Fu, Y. Liu, Y. Ding, et al., Chem. Commun. 50 (2014) 2167–2169.
[27] R.C. Felicio, E. Cavalheiro, E.R. Dockal, Polyhedron 20 (2001) 261–268.
[28] R.H. Bailes, M. Calvin, J. Am. Chem. Soc. 69 (1947) 1886–1893.
[29] M. Hirotsu, M. Kojima, K. Nakajima, et al., Bull. Chem. Soc. Jpn. 69 (1996) 2549–2557.
[30] L.N. Rusere, T. Shalumova, J.M. Tanski, et al., Polyhedron 28 (2009) 3804–3810.
[31] J. Welby, L.N. Rusere, J.M. Tanski, et al., Inorg. Chim. Acta 362 (2009) 1405–1411.
[32] T. Uchida, T. Katsuki, K. Ito, et al., Helv. Chim. Acta 85 (2002) 3078–3089.
[33] Y. Shen, W. Duan, M. Shi, J. Org. Chem. 68 (2003) 1559–1562.
[34] J.F. Ohren, H. Chen, A. Pavlovsky, et al., Nat. Struct. Mol. Biol. 11 (2004) 1192–1197.
[35] J. Sun, Y. Niu, C. Wang, et al., Bioorg. Med. Chem. 24 (2016) 3472–3482.
[36] C. Wang, H. Zhang, F. Xu, et al., Molecules 18 (2013) 6057–6091.
[37] G.L. Reddy, S.K. Guru, M. Srinivas, et al., Eur. J. Med. Chem. 80 (2014) 201–208.
[38] B. Mao, S. Gao, et al., Eur. J. Med. Chem. 129 (2017) 135–150.